ES206
Electromechanical conversion

Command control of an electric motor

Mateus Lopes Ricci
Pedro Guilherme Soares Vieira

February 19, 2021

Contents

1 Introduction

1.1 Objectives

The objective of this report is to design a Matlab program that can simulate the operation of an electric drive of a three-phase synchronous electronic machine, and to carry out the parameterization of the associated inverter and control system. In order to achieve these results, each component will be modeled from the equations studied during the operation and control of synchronous machines, by studying the operating conditions under different circumstances.

The study will be divided into four parts, and for each part relevant performance analyses will be performed. The sequence is shown below:

- Synchronous machine powered in full wave
- Pulse Width Modulation
- Progressive voltage control
- Torque control

1.2 Diagram and characteristics of the machine and the circuit

1.2.1 Scheme

The synchronous machine to be studied is represented in a simple way in the following diagram. It can be seen that it is divided into a CONTROL module and a POWER module. The codes will be designed taking into account the influence of one module on the other according to the operating conditions illustrated in the previous section.

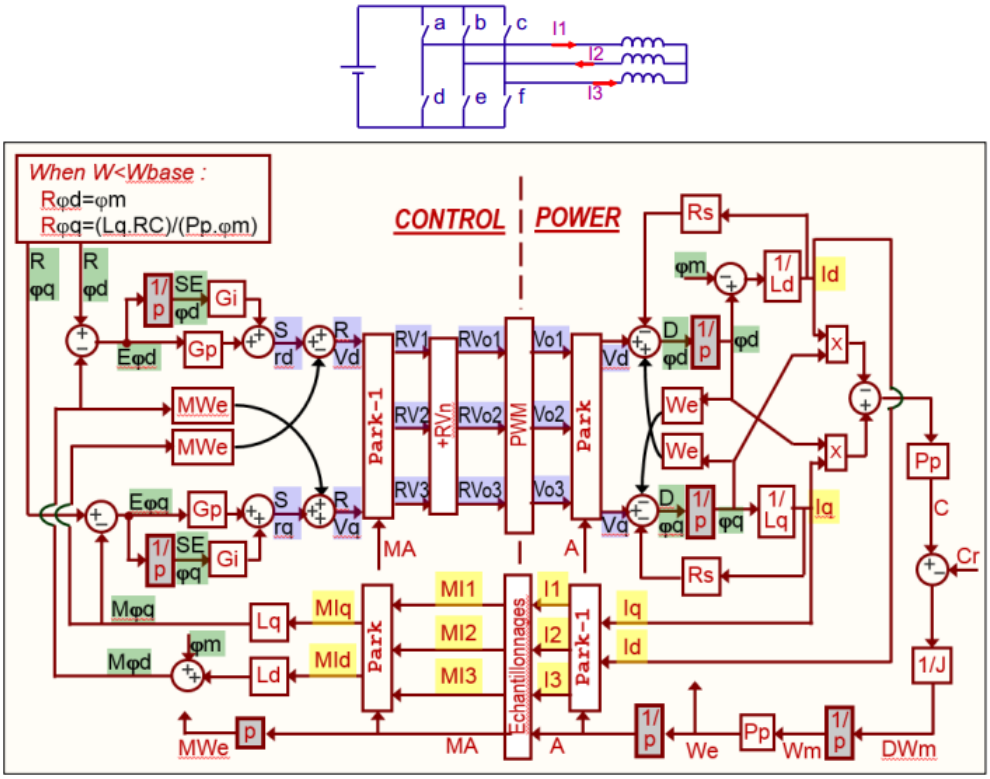

Figure 1.1: Illustrative diagram of the machine and associated electrical circuit.

1.2.2 Characteristics of the machine

The parameters defined below will not be changed during future studies.

- Number of pairs of poles: Pp = 4;
- Stator resistance seen in Park: Rs = 0,18 Ω;
- Direct Park stator inductance: L_d = 1,15 mH;
- Quadratic Park Stator Inductance: L_q = 3,31 mH;
- Flow of magnets seen by all the spirals of a phase: 200 mWb;
- Maximum torque: RC1 = 50 Nm;
- Polar moment of inertia: J = $800 \cdot 10^{-6}$ m^4

The values of the voltages will be different in each evaluated part.

2 Synchronous machine

2.1 General conditions

In this first part, a study focused mainly on the POWER module of the synchronous machine was carried out. For this, the electric machine was considered to be powered by an inverter called full wave, being the voltages out of phase by 120° one from another in time and represented below:

- V_{o1} (i) = E·$sign(sin(\omega_v \cdot t(i) + \pi))$
- V_{o2} (i) = E·$sign(sin(\omega_v \cdot t(i) + \pi\text{-}(2/3)\cdot\pi))$
- V_{o3} (i) = E·$sign(sin(\omega_v \cdot t(i) + \pi\text{-}(4/3)\cdot\pi))$

Where the voltage E is 12 V. A viscous frictional resistive torque k = 0.3 is applied. Calculations for the system power have been made and the results can be seen in the following section. Further details regarding each parameter evaluated can be checked in the description of the respective figures.

2.2 Results

The curves and requested values can be seen in the following figures and table:

Peak current phase 1	25 A
Peak current phase 2	25 A
Peak current phase 3	25 A
Average engine torque	20 N·m
Average speed	69 rad/s
Electrical angle (20 ms)	62°

Table 1: Results of the first part

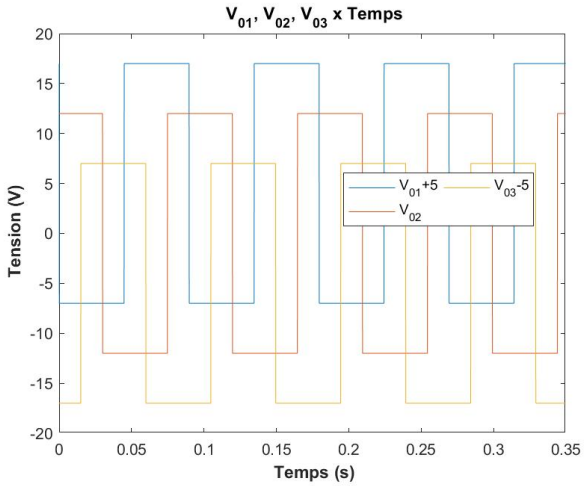

Figure 2.1: Clarke Voltage x Time

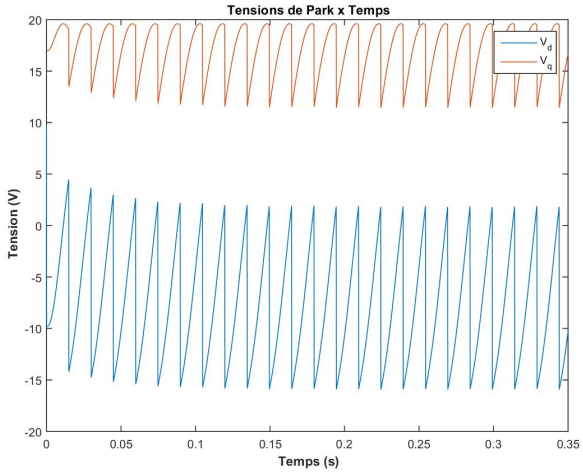

Figure 2.2: Park Voltage x Time

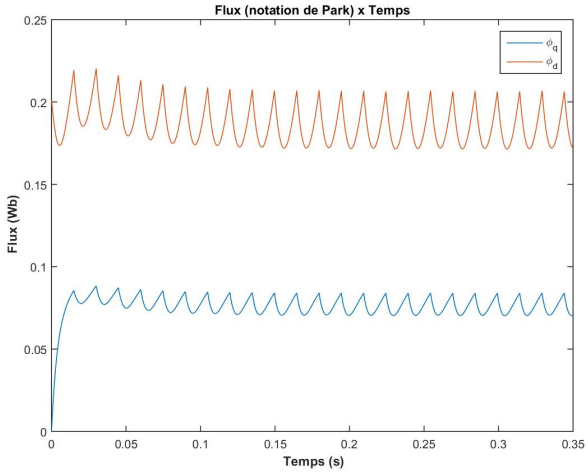

Figure 2.3: Flow (Park notation) x Time

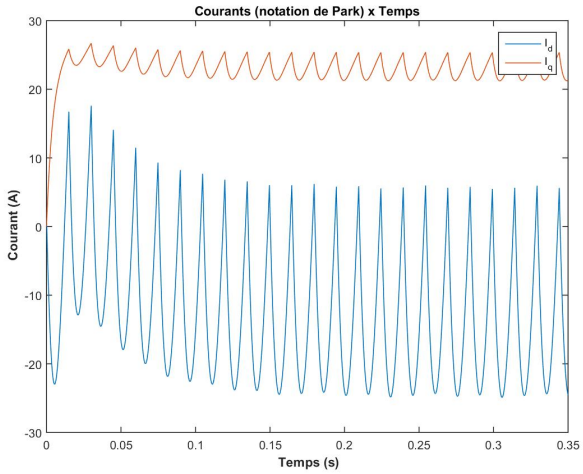

Figure 2.4: Currents (Park notation) x Time

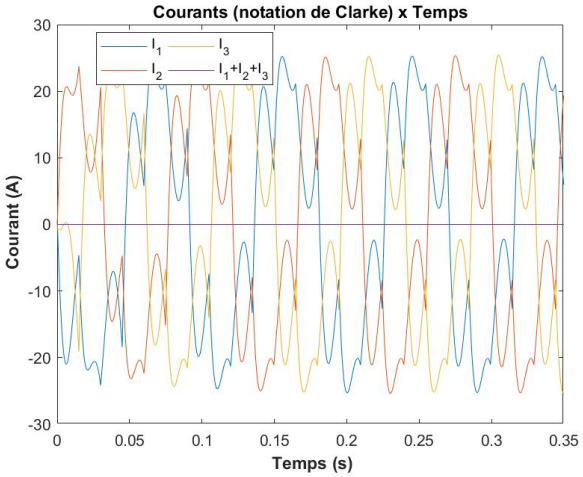

Figure 2.5: Currents (Clarke notation) x Time

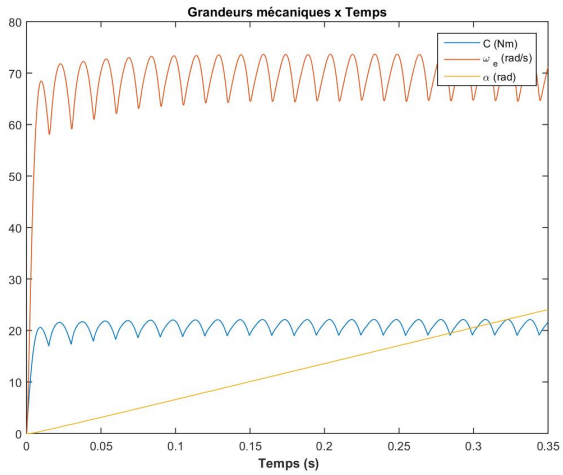

Figure 2.6: Mechanical variables x Time

2.3 Results Analysis

2.3.1 With resistive torque

Diagram 1: The input parameters of this simulation are voltages in square wave format and offset by 120° with respect to each other. To improve visualization, the voltages V_{01} and V_{03} have been shifted by -5V and + 5V respectively.

Diagram 2: Given the need to simplify the mathematical analysis of the problem, the Park transformer was used, reducing the number of voltages in the problem from 3 to 2. Given the Park transformer equation, both DC and quadratic voltages acquire a pulsating profile. It should also be noted that in the period from 0 to 0.1 according to the graph, it exhibits transient behaviour until the subsequent steady-state adjustment.

Diagram 3: It can be observed that the direct and quadratic flow graphs present curves with oscillatory profiles since in their differential equations they are related to Park's voltages, which oscillate in time. Naturally, we can see in the initial part, even around 0.1 seconds, that the curves are in a transient and matching state. This period of transient state represents the time necessary for the system to reach an optimal quadratic flow, close to the maximum possible. After this period, the flows tend to oscillate in smaller intervals but with average values close to the optimal operating values of the machine.

Diagram 4: By considering the expressions used for the calculation of the direct and quadratic currents, it can be verified that the fluxes and currents are linked by constant parameters, such as the respective inductances and the magnetic flux (in the case of the direct flux). Thus, the profiles of the flux curves and Park currents show a rather similar behavior.

Diagram 5: Through the inverse transformation of Park's direct and quadratic currents, 120-degree offseted three-phase currents were obtained, in the same way as three-phase input voltages. As expected, in the initial part, a transient regime is visualized so that they can later be adjusted to the constant oscillation interval. It should also be noted that in the transient and steady state, the sum of the three-phase currents is equal to zero.

Diagram 6: When analyzing the mechanical magnitudes of the problem, both torque and electrical speed have large initial jumps and tend to accommodate a range of oscillations up to steady state. More precisely, the torque increases rapidly until it reaches a value where the electrical torque is very close to the resistive torque. When the difference between the two is small, there is less variation in the electrical speed and, consequently, the torque does the same. It can also be mentioned that in steady state, the torque does not reach the maximum theoretical value, since the maximum operating conditions are not reached, i.e. the mean value of the direct current is not zero and the mean value of the direct flux is less than the magnetic flux. Taking into account the analysis time used, it can be noted that the profile of the electronic angle curve shows a linear behaviour.

2.3.2 No resistive torque

Comparing the two conditions, it can be observed that the suppression of the resistive torque leads to a more unstable system with larger oscillation intervals in all the parameters evaluated, and consequently the system takes longer to reach the steady-state operating regime. As an example, three-phase currents with the resistance factor (coefficient of friction of 0.3) reach steady state around 0.35 seconds. In contrast, the machine without frictional resistance reaches stability at 0.8 seconds.

Thus, it can be seen that the resistive torque functions as a damping factor for the system oscillations, so that the parameters can be adjusted more quickly as soon as the machine is started. In this sense, the removal of this element results in a more unstable and less optimized motor.

3 Pulse Width Modulation

3.1 General conditions

In this second part, it was wished to introduce a pulse width modulator in the inverter in order to make the machine voltages more sinusoidal and to avoid sudden torque changes.

Now the inputs of the system become sinusoidal as follows:

- RV_{o1} (i) = E·$sin(\omega_v \cdot t(i) + \pi)$
- RV_{o2} (i) = E·$sin(\omega_v \cdot t(i) + \pi$-(2/3)·$\pi)$
- RV_{o3} (i) = E·$sin(\omega_v \cdot t(i) + \pi$-(4/3)·$\pi)$

Where the voltage E is 50 V. A viscous friction resistive torque k =0.2 and the cutting period tp =100 μs are applied.

We consider that tr1 is the instant when the voltage V_{01} rises, and tf1 is the instant when it falls. They can be calculated as follows:

- tr1 = tp·(1 - RVo1/E)/4
- tf1 = tp·(3 + RVo1/E)/4

The same applies to the other phases.

3.2 Results

The curves and requested values can be seen in the following figures and table:

Peak current phase 1	41 A
Peak current phase 2	41 A
Peak current phase 3	41 A
Average engine torque	44 N·m
Average speed	22 ·10 rad/s
Electrical angle (20 ms)	212 ·10 °

Table 2: Results of the second part

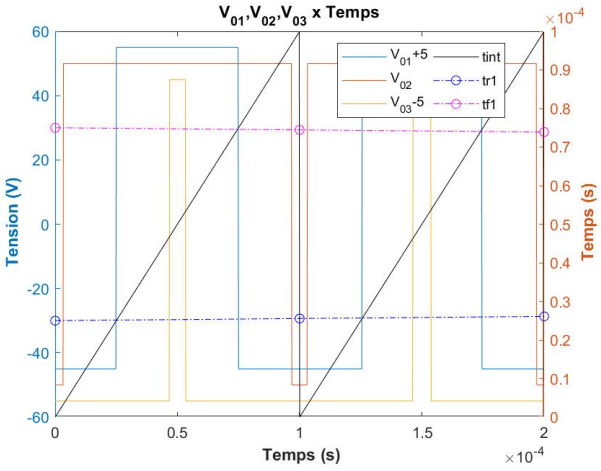

Figure 3.1: Clarke Voltage x Time

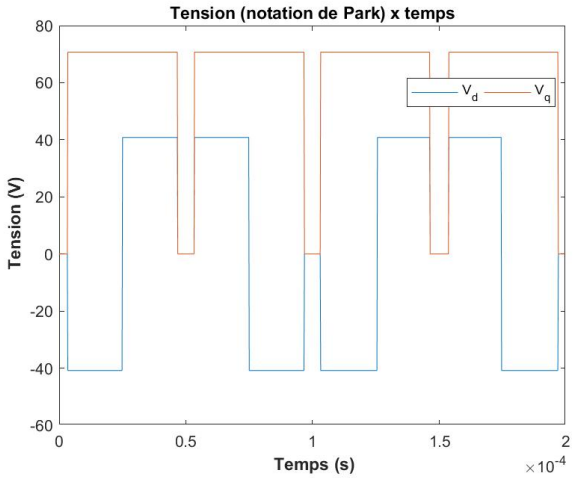

Figure 3.2: Park Voltage x Time

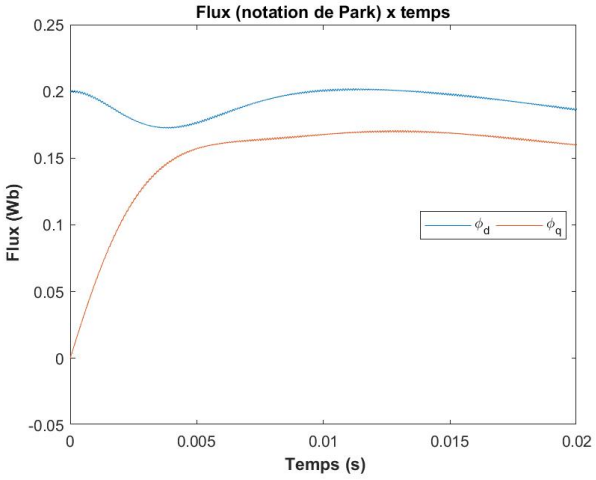

Figure 3.3: Flow (Park notation) x Time

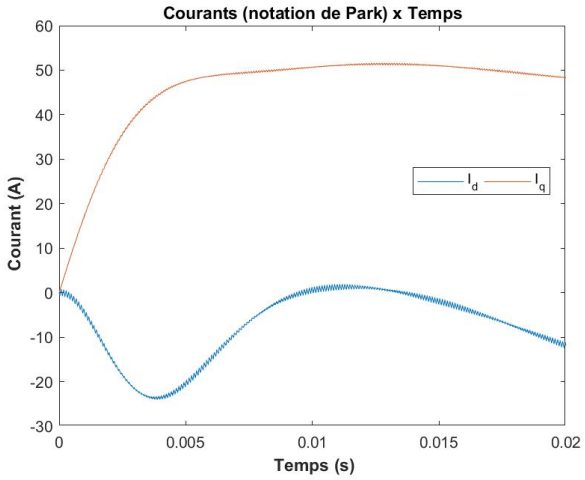

Figure 3.4: Currents (Park notation) x Time

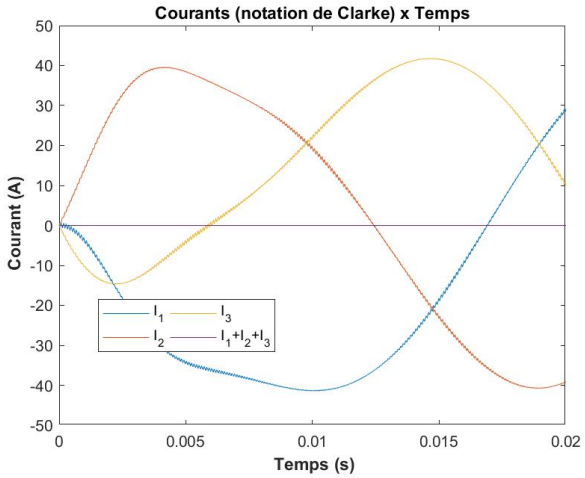

Figure 3.5: Currents (Clarke notation) x Time

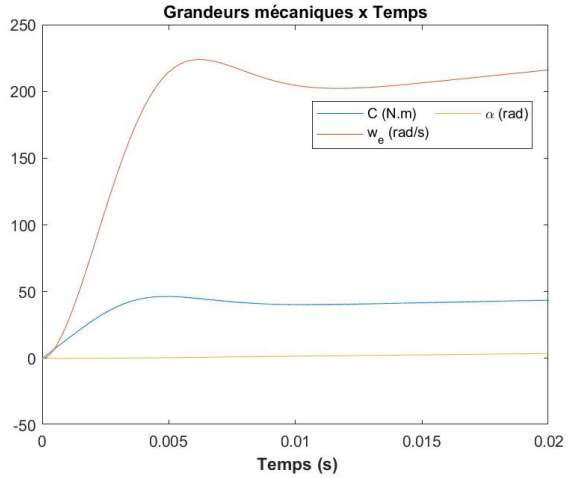

Figure 3.6: Mechanical variables x Time

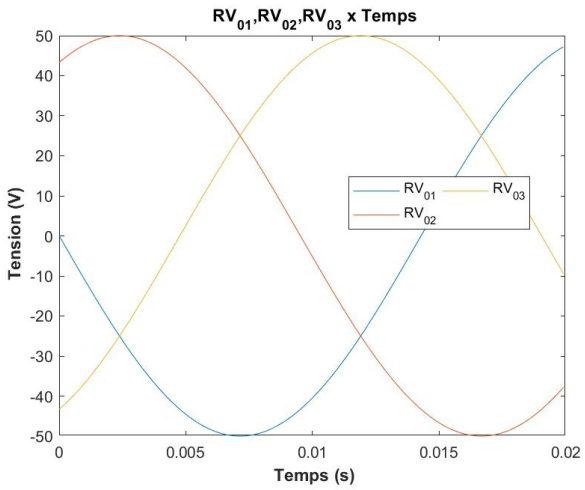

Figure 3.7: $RV_{01}, RV_{02}, RV_{03}$ x Time

3.3 Results Analysis

Diagram 1: By analyzing the voltage curves V_0 for the three phases, it can be seen that the profiles show a change in configuration compared to the same graph in part 1. This change is associated with the modification of the input parameters of the problem which are no longer V_0, but the reference voltages RV_0. By inserting the procedure of voltage regulation by PWM, the voltage V_0 of each phase is regulated by the respective characteristic times (t_r and t_f).

Moreover, for phase 1, it can be seen that for an interval of 1 cutting period, i.e. 0.1 ms, the characteristic times of phase 1 do not change. Furthermore, it is possible to check how the voltage $V0_{01}$ shows a jump to -E and a drop to +E after the respective times t_r and t_f have passed.

Diagram 2: As in part 1, the use of the Park transform simplifies the analysis of the problem. By comparing the previous figure with that of the direct and quadratic constraints, it is possible to see the influence of the characteristic times of the three phases. By analyzing the quadratic voltage profile during the first cut-off period shown at the beginning of the curve, it can be seen that it takes on a zero value, considering that the voltage V_{02} and the phase delay compensate for the other two voltage terms associated with the phases in the expression for calculating the quadratic voltage in the Park transformer. Note that this behavior remains until the respective t_{r2} is reached.

Then, the quadratic voltage jumps and drops in the time period between t_{r3} and t_{f3}, once it jumps to the time corresponding to t_{f2}. After this time, V_q returns to a fall to a value very close to zero.

Diagram 3: When we analyze the curves of the direct and quadratic flows, we can see that the system tends, in the initial phase, to achieve greater stability (by leaving the transient regime). Comparing the flow values with those of part 1, we observe a change in the mean values in steady state, which can be attributed both to the introduction of PWM regulation and to the difference in DC supply voltage.

It can be further verified that PWM brings to the system a greater stability, so that the steady state is reached in a shorter period of time, as well as a greater accommodation of the oscillations, being the flow pulsations contained in smaller intervals.

It is necessary to note that the time in which the system reaches the steady state is not considered in the graphs, since it exceeds the value of 20 ms.

Diagram 4: The direct and quadratic currents have curves quite similar to the curves of the respective flows, since the expressions that link them imply constant parameters, as mentioned earlier. The behaviour along the current curves is explained by the same reasons as those already discussed in the previous analysis.

Diagram 5: Compared to three-phase currents obtained under part 1 conditions, the new currents reach steady-state operation in a shorter time. Another important difference concerns the profile of the curve. The PWM system has allowed a more regular and uniform pulse behaviour.

Diagram 6: As far as the mechanical variables of the synchronous machine are concerned, the PWM system gave the system a satisfactory stability, with much less steady-state oscillations. Another important change is that the new operating conditions result in an average operating torque closer to the maximum possible.

Finally, by comparing the engine torque curve with the profile of the quadratic flow curve, it is possible to verify that the two graphs show a very similar evolution. The same pattern of similarity is observed when the same comparison is made in part 1.

Diagram 7: The graph of the reference voltages shows a regular oscillatory profile with the same pulse, being out of phase by only 120 degrees.

4 Progressive voltage control and monitoring

4.1 General conditions

In this third part, it was wished to introduce a monitoring of the current intensity and a progressive increase of the voltage.

Now the input variables of the system will be RVd and RVq. RV1, RV2, RV3 will be calculated by the Park-1 transformation.

The voltage E is 400 V. A viscous friction resistive torque k =0.1 and the cutting period tp =100 μs are applied.

The industrial system that recovers the measurements at the beginning of each cutting period will be reproduced.

4.2 Results

Peak current phase 1 - (20 ms)	64 A
Peak current phase 2 - (20 ms)	66 A
Peak current phase 3 - (20 ms)	75 A
Maximum engine torque	50 N·m
Average speed	22·10 rad/s
Electrical angle (7 ms)	19°

Table 3: Results of the third part

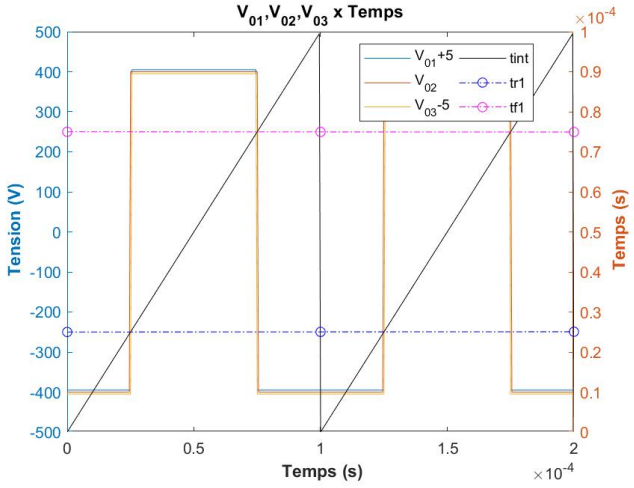

Figure 4.1: Clarke Voltage x Time

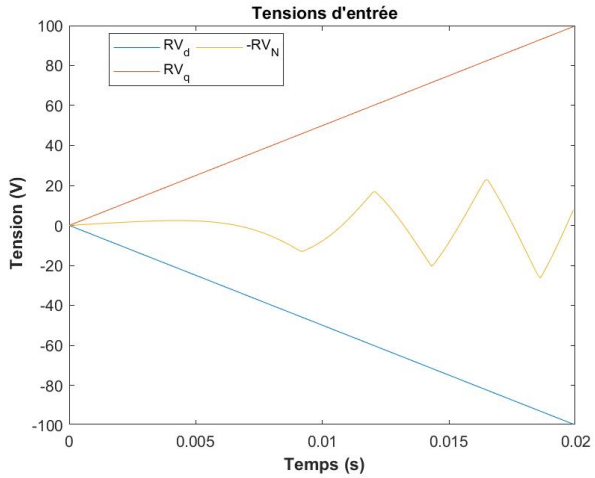

Figure 4.2: RV_d, RV_q, RV_n x Time

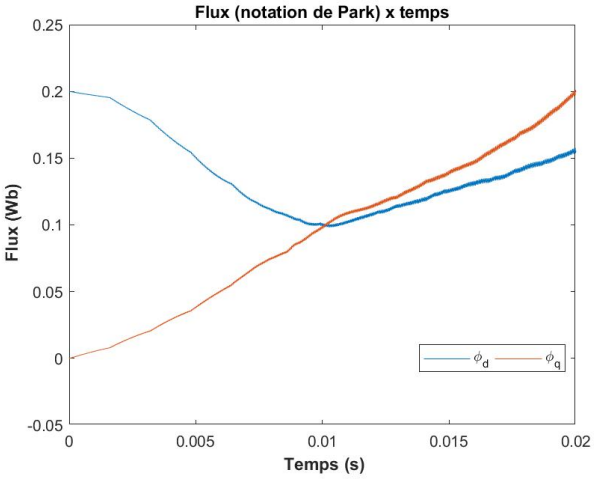

Figure 4.3: Flow (Park notation) x Time

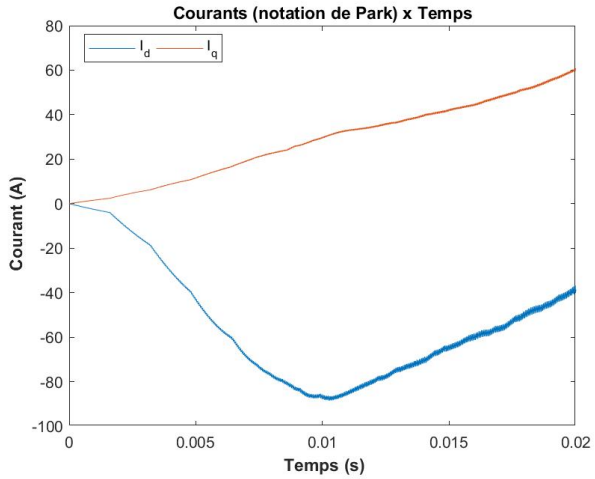

Figure 4.4: Currents (Park notation) x Time

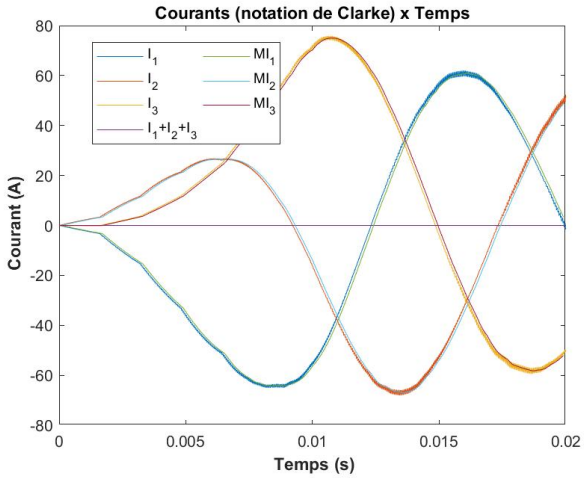

Figure 4.5: Currents (Clarke notation) x Time

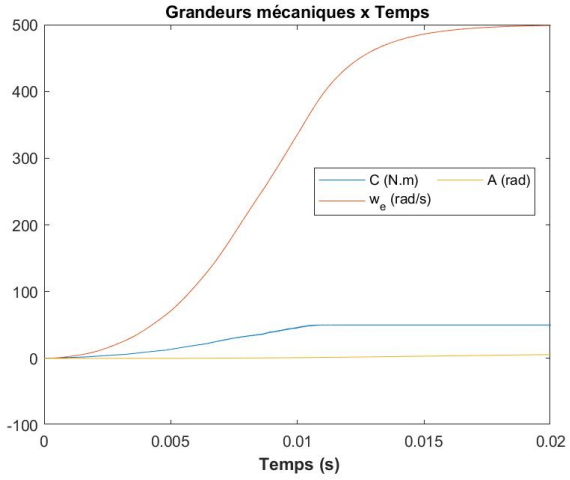

Figure 4.6: Mechanical variables x Time

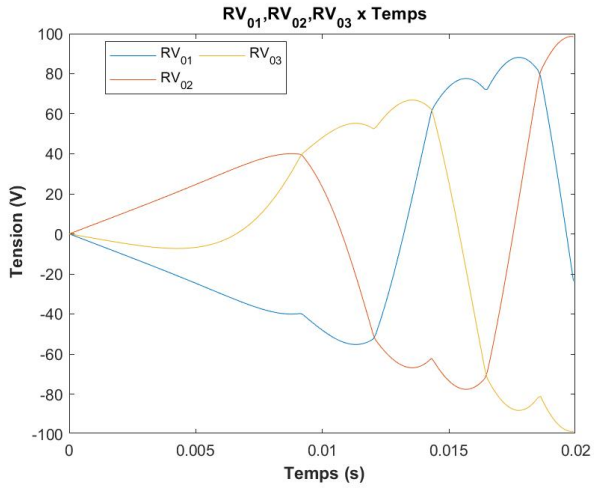

Figure 4.7: $RV_{01}, RV_{02}, RV_{03}$ x Time

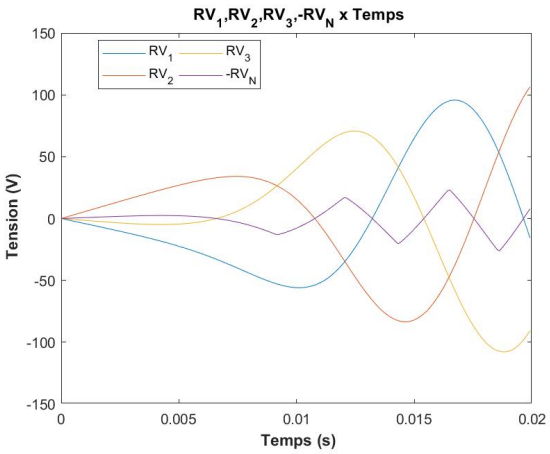

Figure 4.8: $RV_1, RV_2, RV_3, -RV_n$ x Time

4.3 Results Analysis

Diagram 1: When analyzing the oscillator output voltages, the curves show an overlap, which was not observed in part 2. This is due to the fact that in the first cut-off periods, the voltages $\mathrm{RV}_{01,02,03}$ have very low operating values which are very close to each other. Thus, the respective characteristic times of each phase (t_r and t_f) give very similar values.

Diagram 2: The profiles of the direct voltage RV_d and quadratic voltage RV_q curves have a linear and symmetrical behavior, since their input parameters are characterized by being composed of slopes. As for the voltage RV_n, Park's transformer directly influences its calculation. Therefore, the profile of the respective graph follows its equation.

Diagram 3: In this part 3, it is necessary to note that the operating conditions are defined for a range in transient state, and that there is no accommodation and stabilization of some of the parameters evaluated, as it will be possible to observe in the following graphs.

Nevertheless, it can be observed that for the short sampling time, under the new conditions, the quadratic flow goes beyond the direct flow.

Diagram 4: Given the behaviour of the direct and quadratic current curves, it is again possible to find a similarity with the flow curves. Although the quadratic flow increases with time, the respective current also increases. The direct current shows a decrease and then an increase to values close to zero.

Diagram 5: The three-phase current diagram shows the adaptation period when the currents reach their out-of-phase waveforms. In addition to the currents obtained in the power calculations, it is possible in this part to analyze the currents that will be used for the control calculations. The currents $\mathrm{MI}_{1,2,3}$ come from the sampling of currents $\mathrm{I}_{1,2,3}$. This sampling is carried out with a frequency equal to the cutting frequency.

The sum of the currents remains zero, which validates the results obtained.

Diagram 6: By analyzing the relevant mechanical variables, it can be observed that the profile of the electrical angle curve follows the one already observed in the previous parts, showing a regular evolution. As for the electrical torque, comparing the same graph in part 2, we observe a greater delay until it reaches a steady state. The same aspect is observed for the curves relating to the electric speed.

Diagram 7: The $\mathrm{RV}_{01.02.03}$ voltage graph has a direct influence on the $\mathrm{RV}_{1.2.3}$ and RV_n voltages. It can be observed that the time between a minimum and a maximum value of RV_n coincides with the characteristic points of the functions $\mathrm{RV}_{01.02.03}$, which leads to a jump in values.

Diagram 8: The RV voltage graph behaves as expected given the Park transform in the system input parameters (RV_d and RV_q). It is also possible to check a relationship between the voltages $\mathrm{RV}_{1.2.3}$ and the maximum, minimum and average points of the curve $-\mathrm{RV}_q$, a relationship also associated with the phase delay between them.

5 Torque control

5.1 Conditions générales

In this fourth part, it was desired to control the torque in a precise and optimized way. For this, Vd, Vq will no longer be the inputs to the system, but will result from Phid and Phiq flow regulation.

The voltage E is 400 V. A viscous frictional resistive torque k =0.1 and the cutting period tp =100 μs are applied.

Now we want to run the simulation over 7 ms:

- From 0 to 500 microseconds, no voltage is applied to the machine to leave it stationary.
- From 500 microseconds to 1500 microseconds, the torque is continuously increased from zero to the maximum possible torque.
- This maximum torque is applied up to 7 ms.

Since we limit ourselves to the case where we stay below the base speed, we will apply the following equations for the flux command:

$$\begin{cases} RPhid = Phim \\ RPhiq = \dfrac{(Lq * RC)}{(Pp * Phim)} \end{cases} \tag{1}$$

5.2 Résultats

Peak current phase 1 - (20 ms)	51·10 A
Peak current phase 2 - (20 ms)	52·10 A
Peak current phase 3 - (20 ms)	51·10 A
Maximum engine torque	50 N·m
Final speed	14·100 rad/s
Electrical angle (7 ms)	23·10°

Table 4: Results of the fourth part

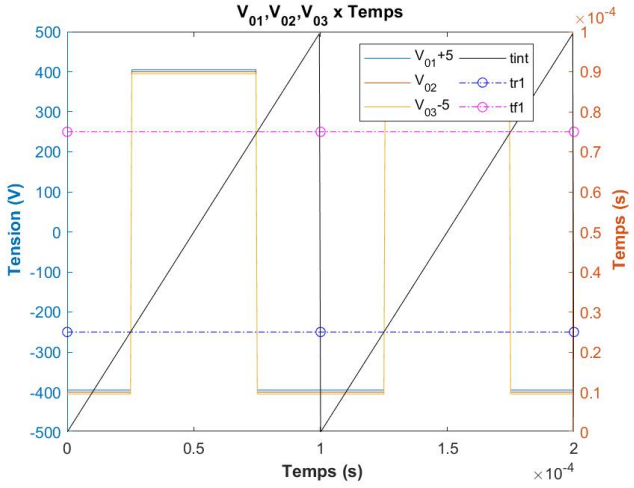

Figure 5.1: Clarke Voltage x Time

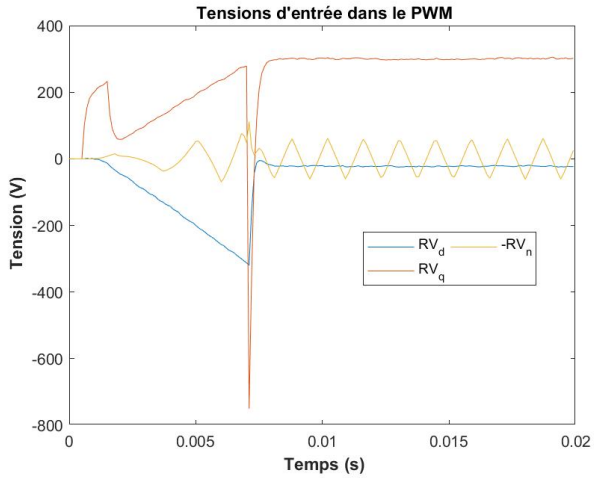

Figure 5.2: RV_d, RV_q, RV_n x Time

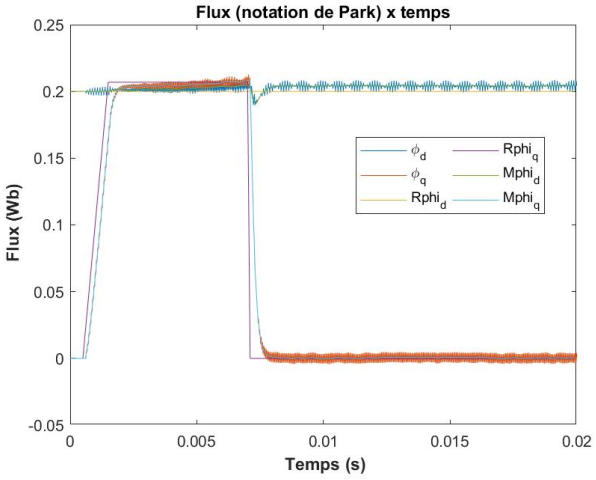

Figure 5.3: Flow (Park notation) x Time

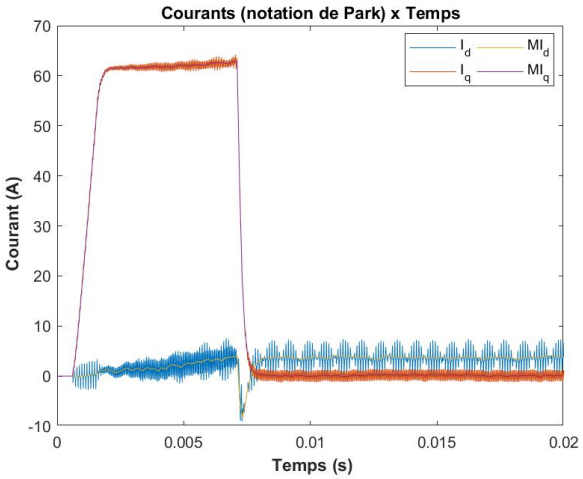

Figure 5.4: Currents (Park notation) x Time

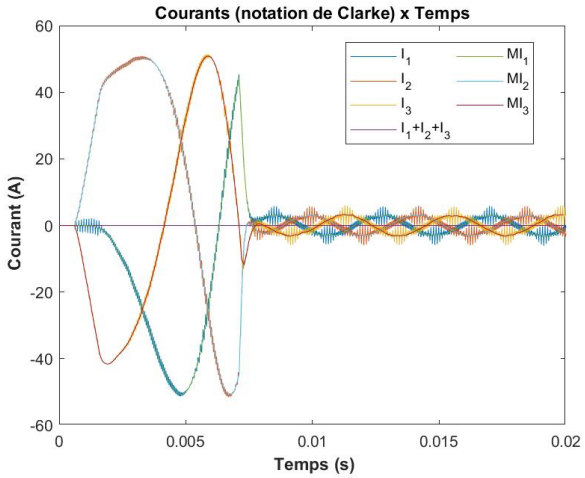

Figure 5.5: Currents (Clarke notation) x Time

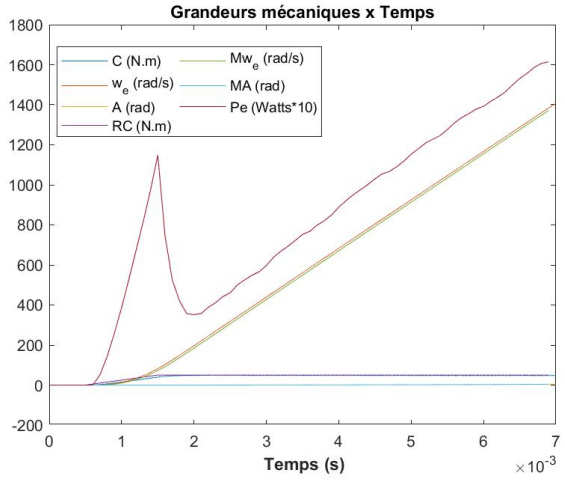

Figure 5.6: Mechanical variables x Time

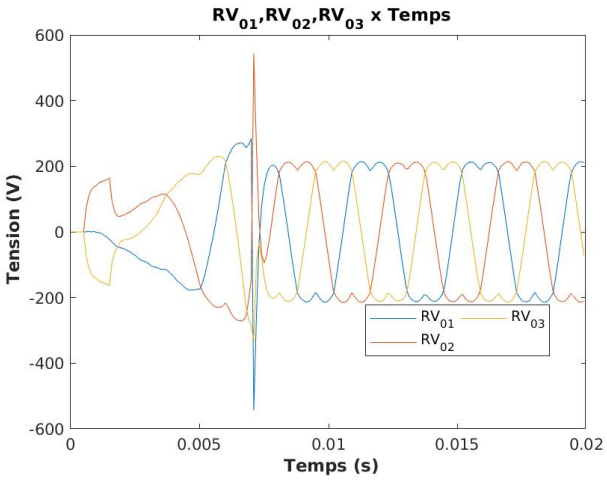

Figure 5.7: $RV_{01}, RV_{02}, RV_{03}$ x Time

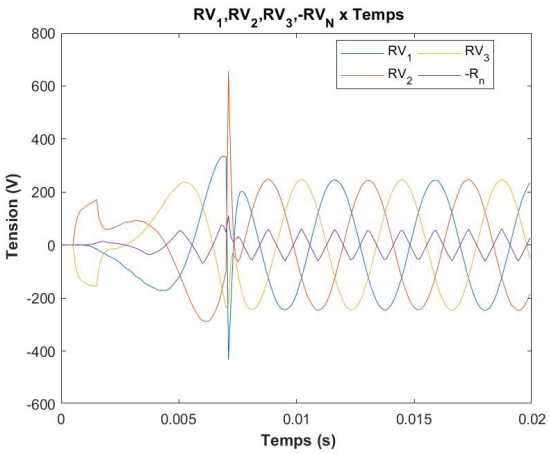

Figure 5.8: $RV_1, RV_2, RV_3, -RV_n$ x Time

5.3 Results Analysis

Diagram 1: The analysis of this diagram is the same as in part 3, since for the first moments of the simulation, the characteristic times of each of the phases have very close values.

Diagram 2: By analyzing the direct voltage RV_d, the quadratic voltage RV_q and the machine neutral voltage RV_n, it is possible to see that from 0 to about 2 ms the voltages have an instability that seems to be transient, but physically this is not true. This unstable phenomenon is the result of a computational artefact, with the objective of obtaining greater stability within a reasonable processing time. This same type of phenomenon can be verified at the moment when the RC reference torque is brought back to zero.

In addition to these aspects, it is possible to verify that the profiles of the curves between 2 and 7 ms are very similar to those observed in the same figure in part 3. From 7 ms, after the calculation artifice, the voltages acquire a fairly regular profile, indicating a permanent operating state.

Diagram 3: With the reference input torque, it is also possible to calculate the direct and quadratic reference flow so that, by successive iterations of the system, the torque reaches the desired value. The curves Mphi_d and Mphi_q are derived from sampling the current values obtained in the power calculations. These values are used to perform control calculations to regulate the torque. At 7 ms, it is possible to see a sudden change in the values of each variable. This variation is due to the fact that the torque input reference value drops to 0.

Diagram 4: By visualizing the figure related to direct and quadratic currents, both those obtained in power and control calculations, the consistency of the results is obvious. It should be noted that because they undergo minor variations in short time intervals, the sample currents show very important oscillations during the moments when the calculation is extensive (0 to 2 ms and about 7 ms), i.e. in the characteristic times highlighted in the analysis of the system's input voltage diagram.

Diagram 5: As in all the other diagrams in this section, it can be seen that until the instant of 1.5 ms, the system remains at rest, since the input reference parameters are zero in this period. From this moment on, the currents increase until they reach values where the torque remains constant. After 7 ms, there is an adaptation period when the reference torque drops to 0, after which the currents remain steady state with smaller amplitudes when the flows reach smaller values.

Diagram 6: Concerning the diagram of mechanical variables, it can be observed that by the implementation of the control mechanism, the system torque tends to follow the evolution of the reference torque. This occurs in the moments of 0.5 ms, 1.5 and 7 ms. In the diagram are also introduced the curves of $\mathrm{M}\omega_e$ and MA which represent the sampling of the values of the electrical speed and the electronic angle.

Diagram 7: Concerning the voltages $\mathrm{RV}_{01.02.03}$ it is possible to notice that there is an adaptation period related to the change of torque by the controller. Then when the reference torque returns to zero, the voltages show a stable variation.

Diagram 8: The $RV_{1.2.3}$ voltage graphs verify the relationship between the maximum voltages of each phase and the system neutral voltage. The instabilities resulting from the calculation artifice are also observed around characteristic times defined for the system operation.

It should also be noted that after the moment when the reference torque takes a zero value and exceeds the moments of instability, the voltages discussed here reach a steady state.

6 Conclusion

The work carried out has made it possible to verify step by step the influence that the addition of mechanisms, both control and power, has on the resulting torques and powers. It is concluded that the operation of the three-phase machine with torque regulator achieves the desired objectives of the project, since it follows, without great delay, the imposed reference parameters.